

Article

Nanomechanical Characterization of Bacterial Polyhydroxyalkanoates Using Atomic Force Microscopy

Simone Bagatella *, Riccardo Ciapponi  and Stefano Turri

Dipartimento di Chimica, Materiali e Ingegneria Chimica “Giulio Natta”, Politecnico di Milano, Piazza Leonardo da Vinci 32, 20133 Milan, Italy; riccardo.ciapponi@polimi.it (R.C.); stefano.turri@polimi.it (S.T.)

* Correspondence: simone.bagatella@polimi.it

Abstract: Polyhydroxyalkanoates are a promising class of biopolymers that can allow the production of sustainable plastic materials. The mechanical properties of such materials are very important for possible industrial applications, but the amount of polymer required for common mechanical testing can be orders of magnitude more than what is possible to achieve with a lab-scale process. Nanoindentation with the Atomic Force Microscope allows an estimation of the Elastic Modulus that can be used as a preliminary measurement on PHA when only a limited amount of material is available. Poly(hydroxybutyrate-co-hydroxyvalerate) copolymers were analyzed, with moduli ranging from 528 ± 62 MPa to 1623 ± 172 MPa, according to both the composition and the crystallization kinetics.

Keywords: AFM; nanoindentation; nanomechanics; elastic modulus; biopolymers; polyhydroxyalkanoates



Citation: Bagatella, S.; Ciapponi, R.; Turri, S. Nanomechanical Characterization of Bacterial Polyhydroxyalkanoates Using Atomic Force Microscopy. *Appl. Sci.* **2022**, *12*, 4994. <https://doi.org/10.3390/app12104994>

Academic Editors: Krzysztof Talaška, Yuri K. Gun'ko, Szymon Wojciechowski and Antoine Ferreira

Received: 11 April 2022

Accepted: 13 May 2022

Published: 15 May 2022

Publisher's Note: MDPI stays neutral with regard to jurisdictional claims in published maps and institutional affiliations.



Copyright: © 2022 by the authors. Licensee MDPI, Basel, Switzerland. This article is an open access article distributed under the terms and conditions of the Creative Commons Attribution (CC BY) license (<https://creativecommons.org/licenses/by/4.0/>).

1. Introduction

Mechanical characterization of materials is fundamental for gaining information about their microstructure and, hence, their possible applicability. Hardness, elasticity, plasticity, strength, and fracture are commonly measured mechanical characteristics. Well-established techniques such as tensile testing, hardness testing, or dynamic mechanical analysis are employed for this purpose [1].

However, since these measurements require macroscopic samples, they cannot be compatible in cases of poor availability of materials. In addition, they mainly provide macroscopic information about the tested samples, and heterogeneities or features at the nano-scale cannot be detected. A solution to these problems is represented by the use of atomic force microscopy (AFM). The AFM, introduced in 1986 and belonging to the scanning probe microscope (SPM) family [2], consists of a micro-machined cantilever probe, a sharp tip mounted to a piezoelectric actuator and a position-sensitive photodiode detector for receiving the reflected laser beam to provide cantilever deflection feedback [3].

AFM spreading over the years is caused by the possibility to analyze the sample, not only obtaining high-resolution topographic images, but also performing a characterization of the nanomechanical properties [4]. In particular, it can provide valuable information on local properties such as elasticity, viscoelasticity, hardness, and adhesion [5–10].

To obtain such information, the so-called force–distance curve must be first obtained through AFM in quasi-static nanoindentation. Force–distance curves can be then fitted with mathematical methods which contain relevant system properties as parameters [3].

This peculiarity caused a strong diffusion of AFM in biology and biomedicine fields, where the understanding of the behavior of complex biological systems is fundamental. In the last decades, AFM was used to evaluate the local elasticity of small, soft, and inhomogeneous samples, such as bacteria, cells but also bone tissues, and a large variety of biomaterials [11–14]. In addition, recent works include the properties investigation of many classes of materials related to different fields of application. By way of example, it is possible

to mention geological materials [15], metallic alloys [16], ceramics [17], polymers [18], nanocomposites [19] and functional nanostructures [20].

Since AFM allows to determine both the microstructure and the local mechanical properties of soft matter, it has been revealed as a particularly interesting tool for probing polymers, whose morphology presents relevant features at the nanoscale [21]. As mentioned above, in the last decade, several pioneering studies using AFM nanomechanical mapping on polymers have been published [22]. Among the large variety of studied polymers, it is possible to cite homopolymers such as polyvinyl acetate, polystyrene or polymethylmethacrylate [23,24], blends like polystyrene/poly(*n*-butyl methacrylate) or polyolefin elastomer/polyamide [25,26], and even polymer-based composites materials [27,28]. In particular, the Elastic modulus is the most diffusely measured parameter, having been quantitatively deduced for several polymeric bulk samples and thin films with elastic modulus varying in a wide range, from a few kPa, e.g., hydrated hyaluronic acid hydrogels, to several GPa, e.g., polymethylmethacrylate, polyethylene naphthalate, or oxidized polyimides [29,30].

It should be mentioned, the use of AFM for the microstructure mechanical investigation of biopolymers. Indeed, the knowledge of the relationships between structure, properties, and performance is essential for prospective safe applications of biodegradable and/or bio-based polymers [31]. Both natural and synthetic biopolymers have been reported in more recent years. Cellulose fibers, polycaprolactone, polyvinyl acetate, polylactic acid (PLA) and cellulose-reinforced starch–gelatin polymer composite are a few of the investigated materials [32–35].

In this work, we propose a nanomechanical characterization by force–distance curves obtained via AFM of different biopolyesters belonging to the broad family of hemisynthetic and bacterial polyhydroxyalkanoates (PHA). Parameters, methodologies and accessibility of AFM tests were studied and described in previous experiences in our research group [30]. First, a comparison of the mechanical properties measured via conventional tensile test and tip nanoindentation AFM test are presented, using polylactic acid (PLA) as a standard. Then, elastic moduli obtained by tip indentation AFM test are shown for different poly(hydroxybutyrate-co-hydroxyvalerate (PHBV) copolymers, obtained by bacterial co-fermentation of different volatile fatty acid mixtures. Finally, a correlation of the obtained elastic modulus with composition, microstructure and thermal properties is proposed.

2. Materials and Methods

2.1. Materials

PHA-rich biomasses from a mixed microbial culture (MMC) selected under feast and famine conditions in a Sequencing Batch Reactor (S-SBR) using volatile fatty acids (VFAs) as substrates were kindly supplied by the Department of Biotechnology of Università di Verona (Prof. N. Frison). The PHA-rich biomass was obtained with VFAs investigating different ratios of acetic acid (HAc) to propionic acid (HPr). In particular, the following proportions were studied: 100:0 HAc:HPr; 60:40 HAc:HPr; 50:50 HAc:HPr; 30:70 HAc:HPr; 0:100 HAc:HPr. PHA samples were obtained by extraction in chloroform and recovered after filtration and drying [36].

As reported in a previous work of ours, the extracted PHA samples resulted to be complex blends of poly(hydroxybutyrate-co-hydroxyvalerate) (PHBV), where different phases, having a well-defined ratio between hydroxybutyrate (HB) and hydroxyvalerate (HV), were present. To investigate the properties of a well-defined PHBV phase, a solvent/non-solvent fractionation was also carried out for an extracted PHA batch [37].

The PHAs samples were then characterized, and the nanomechanical properties were tested by AFM.

As a benchmark for AFM testing, polylactic acid (PLA) Ingeo™ 4043D was supplied by NatureWorks LLC.

2.2. Methods

In the following, the methods used for the materials characterizations are described.

2.2.1. Spin-Coating

The materials were deposited by spin-coating in the form of thin film on a glass substrate to allow AFM characterization. Parameters (400 rpm, 40 s) were set to guarantee a minimum thickness of $\approx 1 \mu\text{m}$, which is required for reliable AFM analysis. At the end of the deposition process, the wet thin films were dried on a stove at $60 \text{ }^\circ\text{C}$ in vacuum condition for at least 40 min to guarantee solvent evaporation and to avoid contamination of the wet film.

2.2.2. Atomic Force Microscopy (AFM)

An AFM NscriptorTM DPN-WriterTM was used to study the morphology and nanomechanical properties of thin films obtained by spin-coating. Data were collected by the software SPM COCKPIT (Pacific Nanotechnology Inc., Santa Clara, CA, USA) and analyzed by OriginPro version 2020 (OriginLab Corporation, Northampton, MA, USA). Force–distance curves were performed in air at 0.05 Hz, with ACT tips from AppNano[®] (Santa Clara, CA, USA) with a nominal radius of curvature less than 10 nm and a half-opening angle of $\alpha = 24^\circ$. Morphological images were taken using ACT-SS (super sharp) tips from AppNano[®] with cantilever stiffness $k_c = 37 \text{ N/m}$, tip radius $r = 6 \text{ nm}$, and half-opening angle $\alpha = 18^\circ$. Scanning was performed over 256 lines, 0.2 lines per second on two different square areas: $50 \times 50 (\mu\text{m})$ and $2 \times 2 (\mu\text{m})$.

2.2.3. Nuclear Magnetic Resonance (NMR)

The PHA compositions were determined using $^1\text{H-NMR}$ spectroscopy. Spectra were recorded in deuteriochloroform (CDCl_3) (10 mg mL^{-1} for $^1\text{H-NMR}$) at $25 \text{ }^\circ\text{C}$ on a Bruker SampleXpress spectrometer. Relative peak intensities for this purpose were analyzed using the peak fitting program MNova. Peak shifts were referenced to the CDCl_3 peak at 7.26 ppm.

2.2.4. Gel Permeation Chromatography (GPC)

Molecular weight measurements on extracted and fractionated PHA samples were performed using a Waters 510 Gel Permeation Chromatography (GPC) apparatus working in tetrahydrofuran (THF) at $40 \text{ }^\circ\text{C}$, equipped with a set of Ultrastyrigel[®] columns and a Waters 410 differential refractometer as a detector. The calibration was performed with monodisperse fractions of polystyrene.

2.2.5. Dilute Solution Viscometry

Dilute solution viscometry was carried out for one extracted PHA batch, insoluble in THF for GPC analysis. The sample was dissolved in CHCl_3 and the efflux time of the solution from a capillary in calibrated glass was measured at $30 \text{ }^\circ\text{C}$. The intrinsic viscosity was computed with a double extrapolation at zero concentration of two semi-empirical equations (Huggins and Kraemer equations). Then, Mark–Houwink’s empirical equation was exploited to obtain the viscosity average molecular weight (M_η) assumed to be equal to the weight average molecular weight M_w as a first approximation. The empirical constants of PHB in CHCl_3 at $30 \text{ }^\circ\text{C}$ were used, with $K = 0.0118 \text{ mL/g}$ and $\alpha = 0.78$ [30].

2.2.6. Differential Scanning Calorimetry (DSC)

Thermal properties analysis was carried out using DSC for extracted and fractionated PHA. Differential scanning calorimetry (DSC) was performed with a DSC 823 e (Mettler-Toledo, Columbus, OH, USA). All runs were performed on 5–10 mg samples in a nitrogen atmosphere. The data obtained were used to measure characteristic temperatures and their enthalpies. The DSC thermal history consisted of: (i) first heating run from $25 \text{ }^\circ\text{C}$ to $200 \text{ }^\circ\text{C}$ ($20 \text{ }^\circ\text{C min}^{-1}$); (ii) cooling step from $200 \text{ }^\circ\text{C}$ to $170 \text{ }^\circ\text{C}$ ($20 \text{ }^\circ\text{C min}^{-1}$), from $170 \text{ }^\circ\text{C}$ to $0 \text{ }^\circ\text{C}$

(10 °C min⁻¹) to stimulate the polymer crystallization, from 0 °C to -50 °C (20 °C min⁻¹); (iii) second heating run from -50 °C to 200 °C (20 °C min⁻¹).

2.2.7. Uniaxial Tensile Tests

PLA tensile properties were determined at room temperature using a Zwick/Roell Z010 (Zwick Roell Italia, Genova, Italy) equipped with a 10 kN load cell and a long-stroke extensometer following the standard test method ASTM D638-14.

3. Results

In this section, surface morphology investigation by AFM in tapping mode, raw data acquisition by tip indentation AFM test, data elaboration, and elastic moduli of the extracted PHA blends are presented. Also, the elastic modulus evolution with time is reported for a fractionated sample of PHA. For further information about PHA materials production methods and compositional, morphological, and thermal characterization, please refer to the previous work [37].

In addition, the validation of the elastic moduli extrapolation is carried out by comparing it with the Elastic modulus measured by conventional tensile test for PLA, used as a benchmark.

3.1. Surface Morphology

When deposited in the form of thin film, PHA samples were transparent to visible light at the macroscopic scale. To isolate homogenous portions of material for the tip indentation AFM test, the surface morphology of the PHA samples was observed.

The PHA morphology was investigated by tapping mode AFM, once deposited by spin-coating on a glass substrate having an arithmetic mean height S_a and a root mean squared height S_q equal to 16.7 nm and 22.8 nm, respectively. Note that 50 × 50 (μm) and 2 × 2 (μm) height and demodulation images are reported in Figure 1.

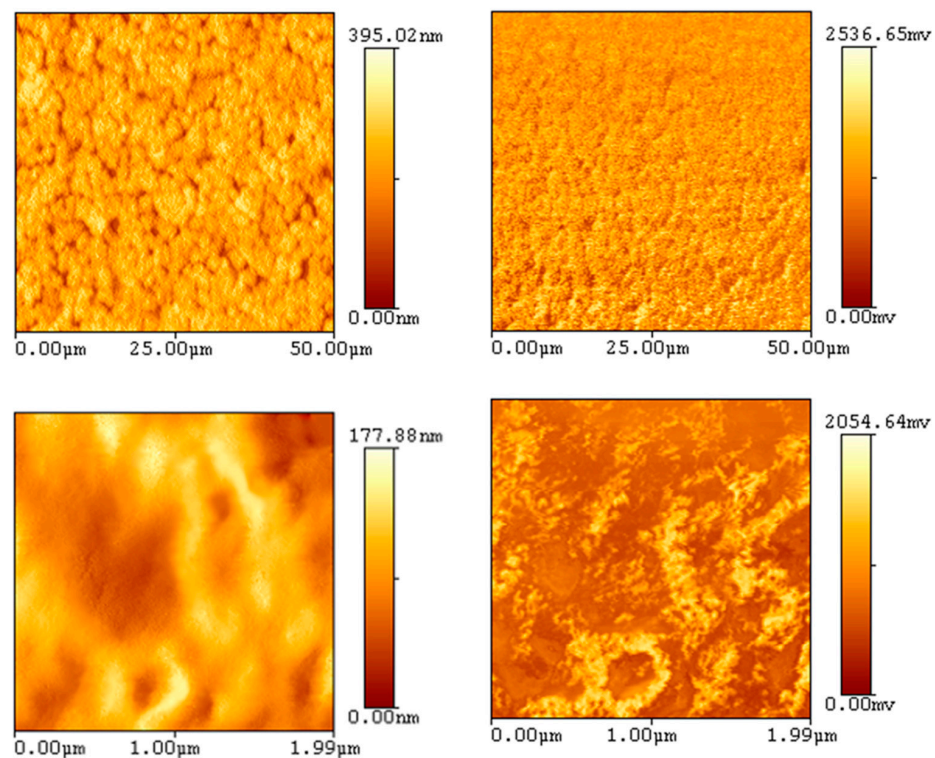


Figure 1. Images of surface morphology acquired by AFM in tapping mode for PHA thin films. (Top): height (left) and demodulation (right) 50 × 50 (μm) images; (bottom): height (left) and demodulation (right) 2 × 2 (μm) images.

The 50 × 50 (μm) height image is coupled with a line profile (Figure 2) to highlight the typical roughness showed by the PHA samples.

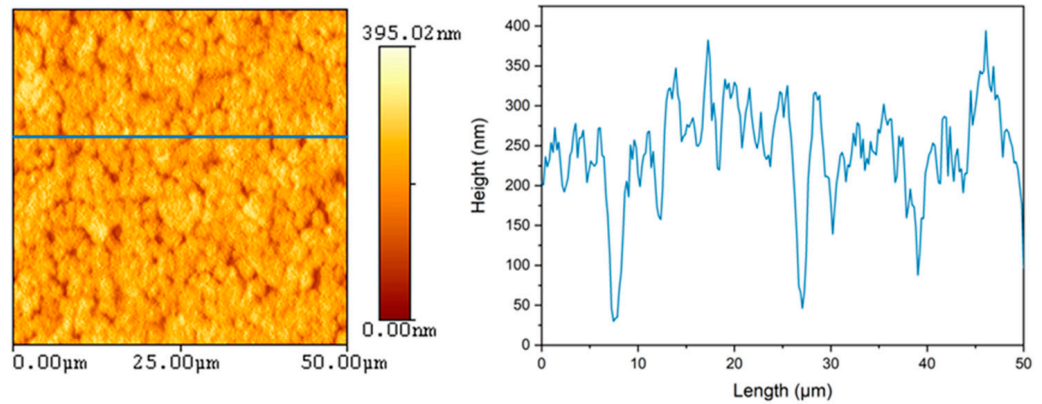


Figure 2. Height 50 × 50 (μm) image of surface morphology acquired by AFM in tapping mode for PHA thin films sample (left) and its line profile (right).

Choosing a reference plane, whose area is A, and defining Z(x,y) as the distance between the points and the reference plane, roughness parameters are defined as follows:

$$S_a = \frac{1}{A} \iint |Z(x,y)| dx dy \tag{1}$$

$$S_q = \sqrt{\frac{1}{A} \iint Z^2(x,y) dx dy} \tag{2}$$

where S_a and S_q are the arithmetic mean height and root mean squared height, respectively. For the surface morphology shown in Figure 2, the surface roughness parameters, specifically the arithmetic mean height S_a and root mean squared height S_q , were calculated. S_a and S_q resulted to be equal to 51.4 nm and 66.2 nm, respectively.

3.2. Raw Data and Data Elaboration

AFM was used to perform force–distance curves, as reported in Figure 3. The cantilevers used in the analyses were calibrated on silicon slabs before the tests on the samples. To evaluate the elastic modulus, the Sneddon model was used [38]. The equation used is the following:

$$F = \frac{2}{\pi} \tan \alpha \frac{E_s}{(1 - \nu_s^2)} \delta^2 \tag{3}$$

where F is the applied force, α is the half-opening of the tip, considered conical in the ending part, E_s and ν_s are the elastic modulus and the Poisson’s ratio of the sample (assumed equal to 0.35), respectively, and δ is the indentation depth, as previously described in other studies [9].

The force was calculated as follows:

$$F = k_c Z_c \tag{4}$$

where k_c is the cantilever spring constant and Z_c is the cantilever deflection.

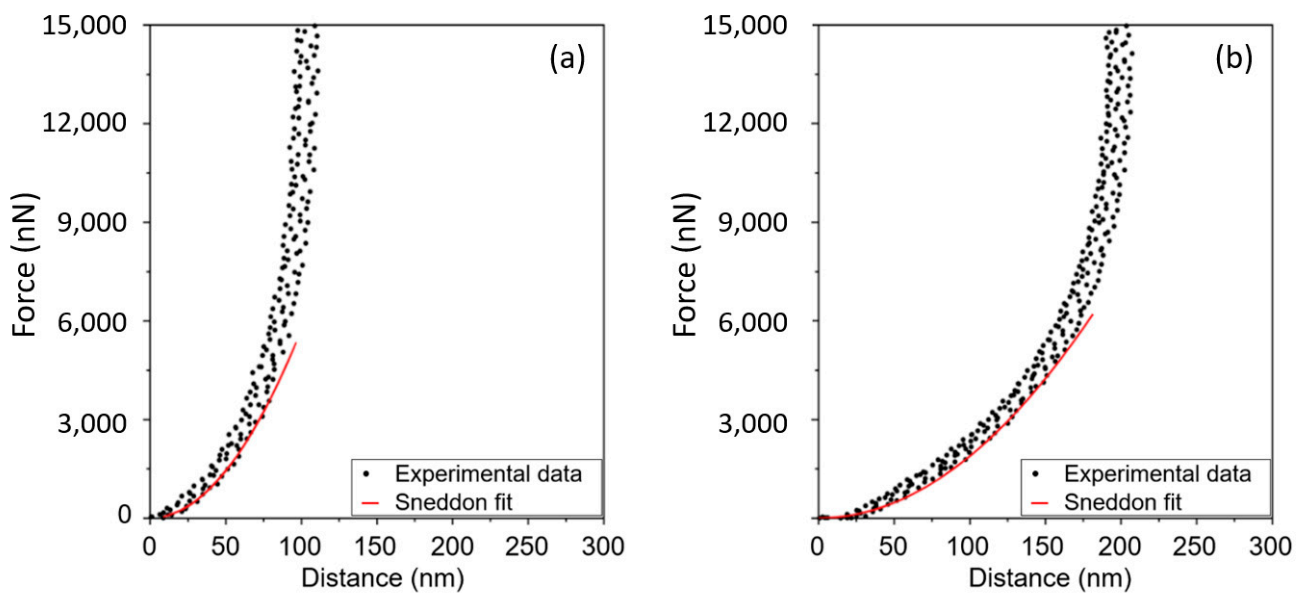


Figure 3. Force–distance curves of the tested bio-polyesters: (a) PLA; (b) P(3 HB-co-88% 3 HV).

The cantilever spring constant was calculated using the Sader method, that for rectangular cantilevers defines k_c as follows [39]:

$$k_c = 0.1906 \rho b^2 L Q \Gamma_i(\omega_R) (\omega_R)^2 \tag{5}$$

where ρ is the density of the fluid surrounding the cantilever, b and L are the cantilever width and length, respectively, ω_R and Q are the radial resonant frequency and quality factor in a fluid of the fundamental flexural mode, respectively, and $\Gamma_i(\omega_R)$ is the imaginary part of the dimensionless hydrodynamic function evaluated at resonant frequency [40]. The quality factor describes the relative width of the resonance peak, and it is equal to the resonant frequency divided by the half-width of the square amplitude resonance peak.

The fitting of the curves was performed with OriginPro 8.5 software. The quality of the fitting was evaluated in terms of the coefficient of correlation R^2 . The adjusted R^2 coefficient was considered a valid measure for the reliability of interpolation, and it is defined by the following equation:

$$\text{adjusted } R^2 = - \frac{\sum_{i=1}^n \frac{(y_i - \hat{y})^2}{(n-k)}}{\sum_{i=1}^n \frac{(y_i - \bar{y})^2}{(n-1)}} \tag{6}$$

where y_i and \hat{y} are the original measured data values and modeled values, respectively, \bar{y} is the mean of the observed data, n is the number of dataset points and k is the number of parameters calculated by the interpolation. Fitting was selected to have adjusted R^2 higher than 0.990.

Every sample had a total of eight indentations at different points, leading to eight force–distance curves, from which the elastic modulus was extrapolated. Figure 3 shows an example of such fittings.

3.3. Comparison between Tensile Test and Tip Indentation AFM Test

To verify the reliability of elastic modulus measurements extrapolated by the nanomechanical properties tested by AFM, as shown in Figure S1, tensile tests with a dynamometer according to the ASTM D638-14 standard were carried out with a commercial PLA sample.

Young’s modulus of 2450 ± 360 MPa for dumbbell-shaped specimens of PLA was obtained from the tensile test. On the other hand, the elastic modulus from the AFM indentation test was estimated to be 2400 ± 324 MPa. This comparison highlighted an

excellent agreement: the tensile property measured by the conventional tensile test was shown to be correspondent to the nanomechanical property extrapolated by the AFM test.

3.4. Elastic Modulus Measurements in PHA

Nanomechanical characterization was carried out on extracted and fractionated PHA. The elastic modulus of the extracted PHA was calculated with force–distance curves data fitting. Table 1 lists elastic moduli extrapolated for the extracted PHA along with the average composition, molecular weights distribution and thermal properties.

Table 1. Extracted PHA molar composition, elastic modulus from AFM force–distance curves on thin film, weight-average molecular weight M_w , polydispersity index and thermal properties.

HAc:HPr	Elastic Modulus	Molar Composition	M_w	Polydispersity Index	Melting Temperatures	Crystallinity Degree
[g-COD/L:g-COD/L]	[MPa]	[HV mol%]	[10^5 Da]		[°C]	[-]
100:0	1623 ± 172	2%	7.47 *	-	173	48%
30:70	528 ± 62	12%	1.95	2.78	174	38%
60:40	693 ± 74	15%	3.06	1.53	95/138/170	55%
0:100	885 ± 176	40%	2.18	1.66	97/132/172	55%
50:50	700 ± 130	47%	2.45	1.33	98/140/175	55%

* M_w estimated by dilute solution viscometry.

The elastic properties of the tested materials are very similar, except the PHA produced with a substrate of 100:0 HAc:HPr. P(3 HB-co-2% 3 HV) showed an elastic modulus of 1623 ± 172 MPa, while all the other PHA samples showed lower values.

The PHA produced with a substrate composition ranging from 60:40 to 0:100 HAc:HPr exhibited similar elastic responses to the indentation tests: elastic moduli ranged between 528 ± 62 MPa and 885 ± 176 MPa, without a specific trend with the HV content, and with an average value of 702 ± 145 MPa.

3.5. Elastic Modulus Evolution with Time of PHA

A nanomechanical characterization was also carried out on a PHA fraction obtained by a solvent/non-solvent fractionation of an extracted PHA sample, to guarantee the strict compositional homogeneity of the material. In particular, P(3 HB-co-88% 3 HV) with HV content of 88 mol% and a single well-defined peak at 106 °C was tested. This analysis allowed the evaluation of the elastic modulus of the pure copolymer P(3 HB-co-88% 3 HV), and not of the native blend of copolymers.

The indentation tests by AFM were performed one, three, and seven days after the deposition of the thin film. Figure 4 shows the elastic moduli extrapolated for P(3 HB-co-88% 3 HV) after one, three and seven days after the deposition of the thin film.

As shown in Figure 4, P(3 HB-co-88% 3 HV) showed an increasing elastic modulus with time. P(3 HB-co-88% 3 HV) after one day exhibited an elastic modulus of 217 ± 31 MPa, which gradually increased to 285 ± 30 MPa after three days and 708 ± 78 MPa after seven days.

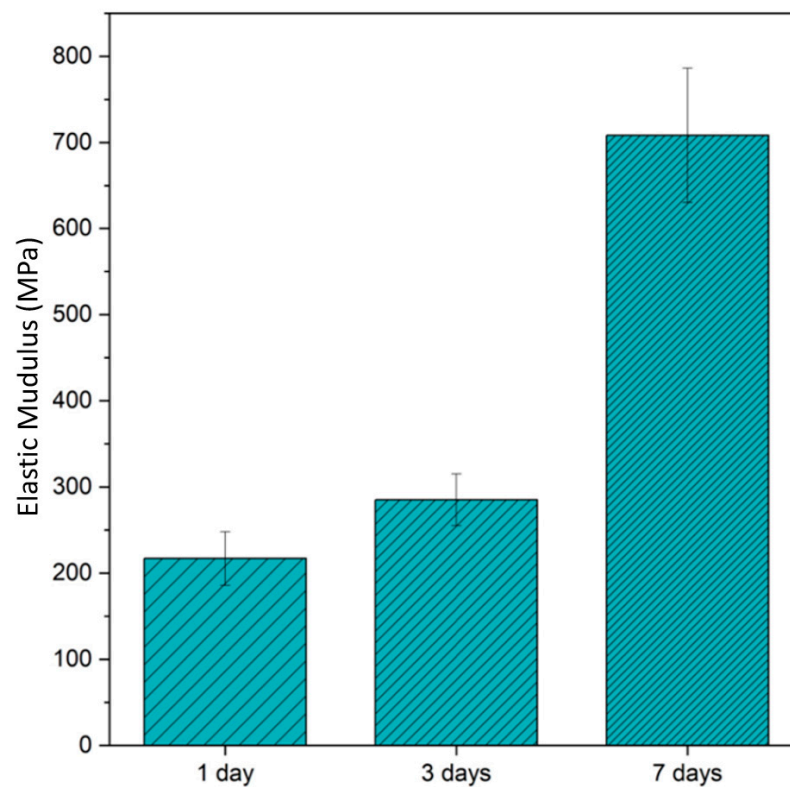


Figure 4. Elastic modulus from AFM force–distance curves of P(3 HB-co-88% 3 HV) one, three, and seven days after the deposition of the thin film.

4. Discussion

In this section, results are discussed in terms of PHA surface morphology, correlation among extrapolated elastic moduli, thermal properties and microstructure of the extracted PHA blends. Also, indirect considerations about crystallization are provided for the fractionated sample of PHA.

4.1. Surface Morphology

The morphology of the PHA surface (Figure 1) appears as small grains, whose size is about 1 μm . The height of those grains is usually between 50 and 100 nm, as it is possible to observe in the line profile of the surface. The demodulation images show no significant phase separation in the samples. This morphology allowed us to carry out indentation tests by AFM.

4.2. Elastic Modulus Measurements in PHA

The PHA produced with a substrate of 100:0 HAc:HPr shows the highest elastic modulus. The latter, indeed, differently from all the others, has a minimal amount of HV units (2 mol%). Therefore, it is reasonable to think that its mechanical properties are not far from those exhibited by poly-3-hydroxybutyrate homopolymer (PHB), which is reported in the literature to have Elastic modulus always above 1 GPa, usually between 1 and 4 GPa [41,42]. In our case, P(3 HB-co-2% 3 HV) shows an elastic modulus of 1623 ± 172 MPa.

All the other PHA samples, having a higher amount of HV units than the case of the PHA produced with a substrate of 100:0 HAc:HPr, show lower and similar values of elastic modulus, without a specific trend. This result is in line with the study of Arcos-Hernández et al. [43], who found that PHBV blends produced by mixed cultures, despite the compositional differences, had similar Elastic modulus, measured by tensile test.

This apparently unexpected behavior can be understood by referring to the crystal phases of the extracted PHA. Despite the compositional variation in terms of HV fraction among the different batches, all PHA highlight three main faster-crystallizing phases,

having similar melting temperatures tested by DSC, and therefore similar compositions. Since mechanical properties tend to be dominated by the properties of the crystalline phases, no large variation of elastic moduli from one batch to another is expected. The only exception is represented by the case of P(3 HB-co-2% 3 HV). This sample, indeed, has a content of HV low enough to exclude the formation of blends, and a single phase rich in HB units.

The main variation of elastic moduli for the extracted PHA, excluding P(3 HB-co-2% 3 HB), can be noticed for the batches produced with 30:70 HAc:HPr and 0:100 HAc:HPr. They show average values of 528 and 885 MPa, respectively, with an average difference of 357 MPa. Such modulus is rather small. However, it must be considered that the crystallization kinetics of each sample is not identical and usually slow. Therefore, it is possible that tests were not performed on materials with a crystallinity fully developed.

4.3. Elastic Modulus Evolution with Time of PHA

The PHA fraction of P(3 HB-co-88% 3 HV) shows an elastic modulus of 708 ± 78 MPa after seven days. This value, as expected, is lower than the elastic modulus usually exhibited by pure PHB: indeed, the increase of HV content allows a reduction of the elastic modulus. For example, in this work, P(3 HB-co-2% 3 HV) shows an elastic modulus of 1623 ± 172 MPa. The introduction of 88 mol% leads to an average reduction of the elastic modulus of 915 MPa.

In addition, the measure of the elastic modulus with time for the PHA fraction, P(3 HB-co-88% 3 HV), allows having indirect information about the crystallization kinetics of this sample. The gradual increase of the elastic modulus with time, from 217 ± 31 MPa after one day, to 708 ± 78 MPa after seven days, suggests that the crystallization kinetics are sluggish. This phenomenon is not uncommon for the PHA [42] and agrees with the thermal analyses. DSC studies, indeed, highlight the absence of crystallization in the second heating scan, indicating a long time required for the copolymer to form crystals [37].

5. Conclusions

A series of PHA with different carbonaceous feeds were analyzed from the nanomechanical point of view and the results were interpreted together with calorimetric results. The AFM proved to be an interesting instrument to evaluate the mechanical properties of PHA when only a small amount of material is available. The results suggest that polymers obtained with a feed of acetic and propionic acid are crystalline and stiff and could be considered for sustainable packaging or other technical applications. By changing the feed-stock of the bacteria that produce PHA, it is possible to modulate the chemical composition of such polymers and obtain a certain degree of variability in the mechanical properties of the extracted PHA.

Supplementary Materials: The following supporting information can be downloaded at: <https://www.mdpi.com/article/10.3390/app12104994/s1>, Figure S1: Example of stress-strain curves for PLA.

Author Contributions: Conceptualization, S.T.; validation, S.B. and R.C.; writing—original draft preparation, S.B.; writing—review and editing, R.C.; supervision, S.T. All authors have read and agreed to the published version of the manuscript.

Funding: This research was funded by the Cariplo Foundation, grant number 2018-0992.

Institutional Review Board Statement: Not applicable.

Informed Consent Statement: Not applicable.

Data Availability Statement: The data presented in this study are available on request from the corresponding author. The data are not publicly available due to privacy.

Acknowledgments: We thank Nicola Frison (Università degli Studi di Verona, Dipartimento di Biotecnologie) for kindly providing us with PHA-rich biomasses. We also thank Elena Ficara (Po-

littecnico di Milano, Dipartimento di Ingegneria Civile e Ambientale) for kindly allowing the PHA extraction from biomasses. This work was funded by the Cariplo Foundation.

Conflicts of Interest: The authors declare no conflict of interest.

References

1. Wiederhorn, S.; Fields, R.; Low, S.; Bahng, G.-W.; Wehrstedt, A.; Hahn, J.; Tomota, Y.; Miyata, T.; Lin, H.; Freeman, B.; et al. Mechanical Properties. In *Springer Handbook of Materials Measurement Methods*; Czichos, H., Saito, T., Smith, L., Eds.; Springer: Berlin/Heidelberg, Germany, 2006; pp. 283–397. ISBN 978-3-540-30300-8.
2. Binnig, G.; Quate, C.F.; Gerber, C. Atomic Force Microscope. *Phys. Rev. Lett.* **1986**, *56*, 930–933. [[CrossRef](#)] [[PubMed](#)]
3. Jalili, N.; Laxminarayana, K. A Review of Atomic Force Microscopy Imaging Systems: Application to Molecular Metrology and Biological Sciences. *Mechatronics* **2004**, *14*, 907–945. [[CrossRef](#)]
4. Garcia, R. Nanomechanical Mapping of Soft Materials with the Atomic Force Microscope: Methods, Theory and Applications. *Chem. Soc. Rev.* **2020**, *49*, 5850–5884. [[CrossRef](#)] [[PubMed](#)]
5. Zemła, J.; Danilkiewicz, J.; Orzechowska, B.; Pabijan, J.; Seweryn, S.; Lekka, M. Atomic Force Microscopy as a Tool for Assessing the Cellular Elasticity and Adhesiveness to Identify Cancer Cells and Tissues. *Semin. Cell Dev. Biol.* **2018**, *73*, 115–124. [[CrossRef](#)]
6. Garcia, P.D.; Garcia, R. Determination of the Elastic Moduli of a Single Cell Cultured on a Rigid Support by Force Microscopy. *Biophys. J.* **2018**, *114*, 2923–2932. [[CrossRef](#)]
7. Chim, Y.H.; Mason, L.M.; Rath, N.; Olson, M.F.; Tassieri, M.; Yin, H. A One-Step Procedure to Probe the Viscoelastic Properties of Cells by Atomic Force Microscopy. *Sci. Rep.* **2018**, *8*, 14462. [[CrossRef](#)]
8. Walker, J.; Umer, J.; Mohammadpour, M.; Theodossades, S.; Bewsher, S.R.; Offner, G.; Bansal, H.; Leighton, M.; Braunstingl, M.; Flesch, H.G. Asperity Level Characterization of Abrasive Wear Using Atomic Force Microscopy. *Proc. R. Soc. A Math. Phys. Eng. Sci.* **2021**, *477*, 20210103. [[CrossRef](#)]
9. Suriano, R.; Ciapponi, R.; Griffini, G.; Levi, M.; Turri, S. Fluorinated Zirconia-Based Sol-Gel Hybrid Coatings on Polycarbonate with High Durability and Improved Scratch Resistance. *Surf. Coat. Technol.* **2017**, *311*, 80–89. [[CrossRef](#)]
10. Ciapponi, R. Sol-Gel Hybrid Fluorinated Coatings: Preparation, Characterisation and Correlation with Human Perceived Sensorial Properties. Master Thesis, Politecnico di Milano, Milano, Italy, 29 April 2015.
11. Chang, K.; Chiang, Y.; Yang, C.; Liou, J. Atomic Force Microscopy in Biology and Biomedicine. *Tzu Chi Med. J.* **2012**, *24*, 162–169. [[CrossRef](#)]
12. Smith, J.R.; Olusanya, T.O.B.; Lamprou, D.A. Characterization of Drug Delivery Vehicles Using Atomic Force Microscopy: Current Status. *Expert Opin. Drug Deliv.* **2018**, *15*, 1211–1221. [[CrossRef](#)]
13. Deng, X.; Xiong, F.; Li, X.; Xiang, B.; Li, Z.; Wu, X.; Guo, C.; Li, X.; Li, Y.; Li, G.; et al. Application of Atomic Force Microscopy in Cancer Research. *J. Nanobiotechnology* **2018**, *16*, 102. [[CrossRef](#)] [[PubMed](#)]
14. Weber, A.; Iturri, J.; Benitez, R.; Toca-Herrera, J.L. Measuring Biomaterials Mechanics with Atomic Force Microscopy. 1. Influence of the Loading Rate and Applied Force (Pyramidal Tips). *Microsc. Res. Tech.* **2019**, *82*, 1392–1400. [[CrossRef](#)] [[PubMed](#)]
15. Wang, K.; Taylor, K.G.; Ma, L. Advancing the Application of Atomic Force Microscopy (AFM) to the Characterization and Quantification of Geological Material Properties. *Int. J. Coal Geol.* **2021**, *247*, 103852. [[CrossRef](#)]
16. Muhammad, H.; Massab, J.; Muhammad, S.; Alkuhayli, A.; Noman, A.M.; Al-Shamma'a, A.A. Indentation Creep Behavior of Pulsed Tungsten Inert Gas Welded Ti-5Al-2.5Sn Alloy Joints by Nanoindentation and Atomic Force Microscopy. *Proc. Inst. Mech. Eng. Part E J. Process Mech. Eng.* **2022**. [[CrossRef](#)]
17. Deng, B.; Luo, J.; Harris, J.T.; Smith, C.M.; Wilkinson, T.M. Toward Revealing Full Atomic Picture of Nanoindentation Deformation Mechanisms in Li₂O-2SiO₂ Glass-Ceramics. *Acta Mater.* **2021**, *208*, 116715. [[CrossRef](#)]
18. Morozov, I.A. Atomic Force Microscopy Nanoindentation Kinetics and Subsurface Visualization of Soft Inhomogeneous Polymer. *Microsc. Res. Tech.* **2021**, *84*, 1959–1966. [[CrossRef](#)]
19. Arora, G.; Pathak, H. Nanoindentation Characterization of Polymer Nanocomposites for Elastic and Viscoelastic Properties: Experimental and Mathematical Approach. *Compos. Part C Open Access* **2021**, *4*, 100103. [[CrossRef](#)]
20. Sobola, D.; Ramazanov, S.; Konečný, M.; Orudzhev, F.; Kaspar, P.; Papež, N.; Knápek, A.; Potoček, M. Complementary SEM-AFM of Swelling Bi-Fe-O Film on HOPG Substrate. *Materials* **2020**, *13*, 2402. [[CrossRef](#)]
21. Collinson, D.W.; Sheridan, R.J.; Palmeri, M.J.; Brinson, L.C. Best Practices and Recommendations for Accurate Nanomechanical Characterization of Heterogeneous Polymer Systems with Atomic Force Microscopy. *Prog. Polym. Sci.* **2021**, *119*, 101420. [[CrossRef](#)]
22. Wang, D.; Russell, T.P. Advances in Atomic Force Microscopy for Probing Polymer Structure and Properties. *Macromolecules* **2018**, *51*, 3–24. [[CrossRef](#)]
23. Stafford, C.M.; Vogt, B.D.; Harrison, C.; Julthongpipit, D.; Huang, R. Elastic Moduli of Ultrathin Amorphous Polymer Films. *Macromolecules* **2006**, *39*, 5095–5099. [[CrossRef](#)]
24. Miyake, K.; Satomi, N.; Sasaki, S. Elastic Modulus of Polystyrene Film from near Surface to Bulk Measured by Nanoindentation Using Atomic Force Microscopy. *Appl. Phys. Lett.* **2006**, *89*, 031925. [[CrossRef](#)]
25. Cappella, B.; Kaliappan, S.K. Determination of Thermomechanical Properties of a Model Polymer Blend. *Macromolecules* **2006**, *39*, 9243–9252. [[CrossRef](#)]

26. Wang, D.; Fujinami, S.; Liu, H.; Nakajima, K.; Nishi, T. Investigation of Reactive Polymer-Polymer Interface Using Nanomechanical Mapping. *Macromolecules* **2010**, *43*, 5521–5523. [[CrossRef](#)]
27. Niu, Y.-F.; Yang, Y.; Gao, S.; Yao, J.-W. Mechanical Mapping of the Interphase in Carbon Fiber Reinforced Poly(Ether-Ether-Ketone) Composites Using Peak Force Atomic Force Microscopy: Interphase Shrinkage under Coupled Ultraviolet and Hydro-Thermal Exposure. *Polym. Test.* **2016**, *55*, 257–260. [[CrossRef](#)]
28. Liang, X.; Ito, M.; Nakajima, K. Reinforcement Mechanism of Carbon Black-filled Rubber Nanocomposite as Revealed by Atomic Force Microscopy Nanomechanics. *Polymers* **2021**, *13*, 3922. [[CrossRef](#)]
29. Passeri, D.; Rossi, M.; Tamburri, E.; Terranova, M.L. Mechanical Characterization of Polymeric Thin Films by Atomic Force Microscopy Based Techniques. *Anal. Bioanal. Chem.* **2013**, *405*, 1463–1478. [[CrossRef](#)]
30. Suriano, R.; Credi, C.; Levi, M.; Turri, S. AFM Nanoscale Indentation in Air of Polymeric and Hybrid Materials with Highly Different Stiffness. *Appl. Surf. Sci.* **2014**, *311*, 558–566. [[CrossRef](#)]
31. Rydz, J.; Šišková, A.; Andicsová Eckstein, A. Scanning Electron Microscopy and Atomic Force Microscopy: Topographic and Dynamical Surface Studies of Blends, Composites, and Hybrid Functional Materials for Sustainable Future. *Adv. Mater. Sci. Eng.* **2019**, *2019*, 6871785. [[CrossRef](#)]
32. Nguyen, H.K.; Fujinami, S.; Nakajima, K. Elastic Modulus of Ultrathin Polymer Films Characterized by Atomic Force Microscopy: The Role of Probe Radius. *Polymer* **2016**, *87*, 114–122. [[CrossRef](#)]
33. Iqbal, Q.; Bernstein, P.; Zhu, Y.; Rahamim, J.; Cebe, P.; Staii, C. Quantitative Analysis of Mechanical and Electrostatic Properties of Poly(Lactic) Acid Fibers and Poly(Lactic) Acid-Carbon Nanotube Composites Using Atomic Force Microscopy. *Nanotechnology* **2015**, *26*, 105702. [[CrossRef](#)] [[PubMed](#)]
34. Chlanda, A.; Kijeńska-Gawrońska, E.; Zdunek, J.; Swieszkowski, W. Internal Nanocrystalline Structure and Stiffness Alterations of Electrospun Polycaprolactone-Based Mats after Six Months of in Vitro Degradation. An Atomic Force Microscopy Assay. *J. Mech. Behav. Biomed. Mater.* **2020**, *101*, 103437. [[CrossRef](#)] [[PubMed](#)]
35. Rodríguez-Castellanos, W.; Flores-Ruiz, F.J.; Martínez-Bustos, F.; Chiñas-Castillo, F.; Espinoza-Beltrán, F.J. Nanomechanical Properties and Thermal Stability of Recycled Cellulose Reinforced Starch-Gelatin Polymer Composite. *J. Appl. Polym. Sci.* **2015**, *132*, 41787. [[CrossRef](#)]
36. Kourmentza, C.; Plácido, J.; Venetsaneas, N.; Burniol-Figols, A.; Varrone, C.; Gavala, H.N.; Reis, M.A.M. Recent Advances and Challenges towards Sustainable Polyhydroxyalkanoate (PHA) Production. *Bioengineering* **2017**, *4*, 55. [[CrossRef](#)] [[PubMed](#)]
37. Bagatella, S.; Ciapponi, R.; Ficara, E.; Frison, N.; Turri, S. Production and Characterization of Polyhydroxyalkanoates from Wastewater via Mixed Microbial Cultures and Microalgae. *Sustainability* **2022**, *14*, 3704. [[CrossRef](#)]
38. Sneddon, I.N. The Relation between Load and Penetration in the Axisymmetric Boussinesq Problem for a Punch of Arbitrary Profile. *Int. J. Eng. Sci.* **1965**, *3*, 47–57. [[CrossRef](#)]
39. Sader, J.E.; Sanelli, J.A.; Adamson, B.D.; Monty, J.P.; Wei, X.; Crawford, S.A.; Friend, J.R.; Marusic, I.; Mulvaney, P.; Bieske, E.J. Spring Constant Calibration of Atomic Force Microscope Cantilevers of Arbitrary Shape. *Rev. Sci. Instrum.* **2012**, *83*, 103705. [[CrossRef](#)]
40. Van Eysden, C.A.; Sader, J.E. Frequency Response of Cantilever Beams Immersed in Viscous Fluids with Applications to the Atomic Force Microscope: Arbitrary Mode Order. *J. Appl. Phys.* **2007**, *101*, 044908. [[CrossRef](#)]
41. Khatami, K.; Perez-Zabaleta, M.; Owusu-Agyeman, I.; Cetecioglu, Z. Waste to Bioplastics: How Close Are We to Sustainable Polyhydroxyalkanoates Production? *Waste Manag.* **2021**, *119*, 374–388. [[CrossRef](#)]
42. Laycock, B.; Halley, P.; Pratt, S.; Werker, A.; Lant, P. The Chemomechanical Properties of Microbial Polyhydroxyalkanoates. *Prog. Polym. Sci.* **2014**, *39*, 397–442. [[CrossRef](#)]
43. Arcos-Hernández, M.V.; Laycock, B.; Donose, B.C.; Pratt, S.; Halley, P.; Al-Luaibi, S.; Werker, A.; Lant, P.A. Physicochemical and Mechanical Properties of Mixed Culture Polyhydroxyalkanoate (PHBV). *Eur. Polym. J.* **2013**, *49*, 904–913. [[CrossRef](#)]